SECURITY CLASSIFICATION OF THIS PAGE

REPORT DOCUMENTATION PAGE

1a. REPORT SECURITY CLASSIFICATION UNCLASSIFIED	1b. RESTRICTIVE MARKINGS
2a. SECURITY CLASSIFICATION AUTHORITY	3. DISTRIBUTION / AVAILABILITY OF REPORT Approved for public release; distribution unlimited.
2b. DECLASSIFICATION / DOWNGRADING SCHEDULE	
4. PERFORMING ORGANIZATION REPORT NUMBER(S) NRL Memorandum Report 6038	5. MONITORING ORGANIZATION REPORT NUMBER(S)
6a. NAME OF PERFORMING ORGANIZATION Naval Research Laboratory 6b. OFFICE SYMBOL (*If applicable*) Code 4420	7a. NAME OF MONITORING ORGANIZATION
6c. ADDRESS (*City, State, and ZIP Code*) Washington, DC 20375-5000	7b. ADDRESS (*City, State, and ZIP Code*)
8a. NAME OF FUNDING / SPONSORING ORGANIZATION Office of the Chief of Naval Research 8b. OFFICE SYMBOL (*If applicable*)	9. PROCUREMENT INSTRUMENT IDENTIFICATION NUMBER
8c. ADDRESS (*City, State, and ZIP Code*) Arlington, VA 22217	10. SOURCE OF FUNDING NUMBERS PROGRAM ELEMENT NO. 61153N; PROJECT NO. RR-023 01-41; TASK NO.; WORK UNIT ACCESSION NO. DD380-021

11. TITLE (*Include Security Classification*)

Foam Generation and Air Entrainment Near a Free Surface

12. PERSONAL AUTHOR(S) Hubbard, D.W., Griffin, O.M., and Peltzer, R.D.

13a. TYPE OF REPORT	13b. TIME COVERED	14. DATE OF REPORT (*Year, Month, Day*)	15. PAGE COUNT
Interim	FROM 10/85 TO 4/87	1987 September 30	38

16. SUPPLEMENTARY NOTATION

17. COSATI CODES			18. SUBJECT TERMS (*Continue on reverse if necessary and identify by block number*)
FIELD	GROUP	SUB-GROUP	(See page ii)

19. ABSTRACT (*Continue on reverse if necessary and identify by block number*)

The flow in a breaking wave is a type of agitation which is conducive to foam formation. The downstream wake of a surface vessel in the seaway also is characterized by a layer of foamy, agitated water near the surface, and a subsurface layer of bubbles or a bubble cloud. The purpose of this report is to discuss the basic features of foam and bubble formation, and air entrainment as these features are known at the present time. We shall discuss possible means for relating these basic features to the processes of deep water wave breaking and of wake formation and development for surface ships moving in the seaway.

20. DISTRIBUTION / AVAILABILITY OF ABSTRACT	21. ABSTRACT SECURITY CLASSIFICATION	
☒ UNCLASSIFIED/UNLIMITED ☐ SAME AS RPT. ☐ DTIC USERS	UNCLASSIFIED	
22a. NAME OF RESPONSIBLE INDIVIDUAL O. M. Griffin	22b. TELEPHONE (*Include Area Code*) (202) 767-2904	22c. OFFICE SYMBOL Code 4420

DD FORM 1473, 84 MAR 83 APR edition may be used until exhausted. All other editions are obsolete.

SECURITY CLASSIFICATION OF THIS PAGE

18. SUBJECT TERMS

Surface foam	Surfactants breaking waves
Bubbles	Ship wakes
Air entrainment	Marine hydrodnamics

Naval Research Laboratory
Washington, DC 20375-5000

NRL Memorandum Report 6038

LIBRARY
RESEARCH REPORTS DIVISION
NAVAL POSTGRADUATE SCHOOL
MONTEREY, CALIFORNIA 93940

Foam Generation and Air Entrainment Near a Free Surface

D. W. HUBBARD

Department of Chemistry and Chemical Engineering
Michigan Technological University

O. M. GRIFFIN AND R. D. PELTZER

Laboratory for Computational Physics
and Fluid Dynamics

September 30, 1987

Approved for public release; distribution unlimited.

CONTENTS

FOAM GENERATION AND AIR ENTRAINMENT NEAR A FREE SURFACE

INTRODUCTION

The flow in a breaking deep water wave is a type of agitation which is conducive to foam formation. The downstream wake of a surface vessel moving in the seaway also is characterized by a layer of foamy, agitated water near the surface, and a subsurface layer of bubbles or a bubble cloud. An extensive study of ship wakes and white water dating from the years during and just after World War Two is given in a U.S. Navy report compiled by the National Defense Research Council (1969). More recently two studies have been conducted at NRL to define more clearly the white-water region of a surface ship wake (Peltzer, 1984; Peltzer, Garrett and Smith, 1987). The highly agitated region of white water just downstream from a typical surface ship is shown in Fig. 1.

The purpose of this report is to discuss the basic features of foam and bubble formation, and air entrainment as these features are known at the present time. We shall discuss possible means for relating these basic features to the processes of deep water wave breaking and of wake formation and development for surface ships moving in the seaway.

PROPERTIES OF FOAM AND BUBBLES

A foam is a coarse dispersion of gas in a liquid, with most of the volume being gas. The liquid is in thin sheets or lamellae between gas bubbles. Foams are formed by dispersing gas into a liquid either by reducing the pressure over the liquid containing a dissolved gas, or by mechanical gas-liquid contact. Mechanical contact can be accomplished by pumping gas through a porous septum or a capillary, or by strongly agitating the liquid. There must be some form of stabilizer or surfactant material present if the foam is not to break or collapse immediately. This means that foams cannot be formed from pure liquids. The foamy region of a highly agitated breaking wave or surface wake region is confined to the near-surface bubbly region. The remainder of the bubble distribution or cloud extends to greater depths due to the turbulent motion of the water.

DeVries (1972) describes the structure of foams. If the foam contains spherical bubbles, up to 74 percent of the foam can be gas if the bubbles have a distribution of sizes. The surface area A of the gas-liquid interface is given by

$$\frac{A}{V_L} = \left[\frac{\Sigma n_i d_i^2}{\Sigma\, n_i d_i^3}\right] \left[\frac{V_G}{V_L}\right] f, \tag{1}$$

where d_i = bubble diameter;
n_i = number of bubbles of diameter d_i;
f = shape factor;
V_G = volume of gas in the foam;
V_L = volume of liquid in the foam.

Manuscript approved April 28, 1987.

Fig. 1 — A typical aerial view of the white water region behind a surface ship underway; from Peltzer (1984)

The factor ($\Sigma\, n_i d_i^2 / \Sigma\, n_i d_i^3$) is the reciprocal of the mean bubble diameter, which depends on the bubble size distribution. As a foam ages, the liquid drains from between the bubbles, and the bubbles begin to coalesce. This causes the surface area, A, to decrease with time.

As the liquid drains, the bubble walls become thin, and the bubbles become polyhedral. Then the lamellae separating them are distorted because of surface tension effects. Pressure differences exist across strongly curved interfaces, so that

$$\Delta p = \gamma \left[\frac{1}{R_1} + \frac{1}{R_2} \right], \tag{2}$$

where γ = surface tension
R_1, R_2 = principal radii of curvature of the interface.

There are illustrations of the meaning of the principal radii in Fig. 2 for two isolated spherical bubbles, and in Fig. 3 for two bubbles which have a very thin lamella between them. It is observed that in foams having polyhedral bubbles, the bubble walls meet in threes, and each angle is 120. This angle does not depend on bubble size or on bubble size distribution. The reason suggested is that the pressure difference between bubbles is determined mainly by the smallest radius of curvature.

The liquid in a foam is located in the so-called plateau borders where the walls of the polyhedral bubbles join. This is illustrated in Fig. 4. Gravity forces and capillary suction can produce very complicated flow patterns in the bubble walls as liquid drains from the foam. The cross-sectional area for flow through the plateau borders in a foam having dodecahedral bubbles is

$$A_{pb} = \left(\sqrt{3} - \frac{\pi}{2} \right) R_1^2 + R_1 \theta \sqrt{3} + \frac{\sqrt{3}}{4} \theta^2. \tag{3}$$

The notation here is that used in Fig. 4. The gas-liquid ratio for this situation is

$$\frac{V_L}{V_G} = \frac{60 A_{Pb}}{2.445\, \pi} \frac{\Sigma\, n_i d_i}{\Sigma\, n_i d_i^3} + 3\theta \frac{\Sigma\, n_i d_i^2}{\Sigma\, n_i d_i^3}. \tag{4}$$

Here d_i is the diameter of a spherical bubble before it becomes a dodecahedron.

The bubble size distribution is an important factor used in describing the structure of foams. This can be measured experimentally by determining the frequency distribution of bubble sizes photographically in a plane passing through the foam. To produce such a plane, the foam can be placed in a container having a flat, transparent wall or the foam can be frozen and part of it sliced away. It has been shown that the size distribution is the same in any plane in a foam, because the bubbles are randomly distributed. The frequency distribution of bubble sizes observed in a plane will differ by a constant from the frequency distribution over a certain foam volume. This is discussed by deVries and Lemlich (1972). The two frequency distribution functions are related by

$$n_s f(r) dr = 2 r C_s N F(r) dr, \tag{5}$$

where n_s = number of bubbles per unit area of the plane;
N = number of bubbles per unit volume in the foam;
$f(r)$ = size distribution function for the plane;
$F(r)$ = size distribution function for the foam volume;
r = bubble radius.

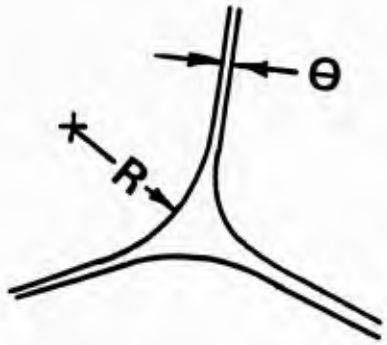

Fig. 2 — Interference geometry for spherical bubbles

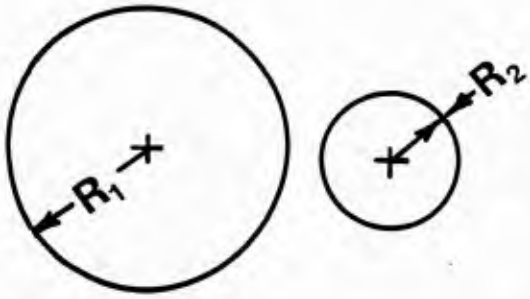

Fig. 3 — Interference geometry for bubbles close together with a thin lamella

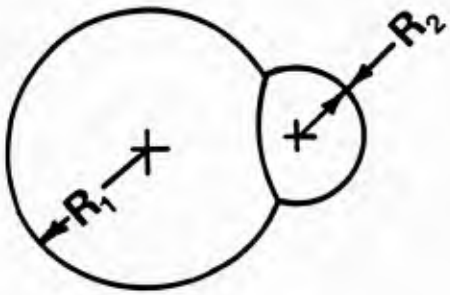

Fig. 4 — Plateau border geometry

Integrating between $r = 0$ and $r = \infty$ relates n_s and N to the mean bubble radius $<r>$,

$$n_s = 2C_s N <r>. \tag{6}$$

The frequency distributions are related by

$$f(r) = \frac{r}{<r>} F(r). \tag{7}$$

The constant C_s can be related to the mean bubble volume, $(4\pi/3) <r^3>$, by

$$n_s = 2C_s N <r> = \frac{3C_s}{\pi} \left[\frac{V_G}{V_G + V_L} \right] \frac{<r>}{<r^3>}, \tag{8}$$

or

$$C_s = \frac{2 \pi N_s <r_s^2>}{3} \left[\frac{V_G + V_L}{V_G} \right], \tag{9}$$

where r_s = radius of bubbles measured directly in a plane. Equation (9) can be used to calculate C_s which depends only slightly on time even though $<r>$ is a function of time due to bubble coalescence. No experimental data are given in the paper by deVries, but some references are given by Lemlich (1972).

Cheng and Lemlich (1983) studied errors which may occur when the bubble size distribution in a foam is measured visually at a plane boundary of the foam. They discuss some effects of statistical bias, bubble distortion by a solid contact plane, bubble segregation at a solid contact plane, and differences in stability of bubbles of different sizes. Planimetric area measurements were compared with longest chord and longest median measurements. The planimetric measurements were found to be the most reliable and were in good agreement with the true bubble size distribution for *homogeneous* new foams. For heterogeneous foams, all methods underestimate the true mean bubble diameter. The main reason seems to be that the small bubbles wedge themselves between the large bubbles and the solid boundary plane, thus pushing them away from the wall. These authors write Eq. (7) as

$$F(r) = \frac{\left[\frac{f(r)}{r} \right]}{\int_0^\infty \left[\frac{f(r)}{r} \right] dr}. \tag{10}$$

The mean bubble radius for a foam can be determined by calculating the moments of the bubble size distribution as

$$r_{j,k} = \frac{\int_0^\infty r^j F(r) dr^{\frac{1}{j-k}}}{\int_0^\infty r^k F(r) dr}. \tag{11}$$

For the biased distribution measured at the boundary surface,

$$r_{s,j-1,k-1} = \frac{\int_0^\infty r^{j-1} f(r) dr}{\int_0^\infty r^{k-1} f(r) dr}^{\frac{1}{j-k}}. \tag{12}$$

The integrals are usually approximated by sums when the mean radii are calculated from experimental measurements. The unbiased and biased mean radii are related by

$$r_{j,k} = r_{s,j-1,k-1}. \tag{13}$$

These last four equations are written using the notation of Cheng and Lemlich (1983).

These authors generated foams with known bubble size distributions and measured the mean radius by observing the foam through a glass boundary. They found that the sizes of bubbles observed in the pool of liquid below the foam corresponded closely to the true sizes of the bubbles in the foam. That is,

$$r_{1,0,P} = r_{1,0,f} \text{ and } S_p = S_f. \tag{14}$$

Their data show that as the range of bubble sizes present becomes larger, the deviation between the true mean bubble size and the mean bubble size measured at the boundary plane also becomes larger. They present their results graphically, and remark that the graphs can be used to predict the error inherent to bubble size measurements made through a boundary wall. These results are shown in Fig. 5 where the ratio of observed to true mean bubble radius is plotted as a function of the observed standard deviation of the bubble sizes made dimensionless using the observed mean bubble radius. Figure 6 shows the relationship between the true standard deviation and the observed standard deviation. All these results are for newly formed foams. In these figures, the notation is as follows:

$r_{s,0,-1,f}$	= Mean bubble radius in foam measured at the boundary surface;
$r_{1,0,P}$	= Mean bubble radius in the pool of liquid below the foam;
$r_{1,0,f}$	= True mean bubble radius in the foam;
S_P	= Standard deviation for bubble sizes in the pool of liquid below the foam;
$S_{s,f}$	= Standard derivation for bubble sizes measured in foam measured at the boundary surface.

Desai and Kumar (1983) studied liquid hold-up in foams which were formed in a polymethyl methacrylate cylinder by blowing air continuously through a pool of liquid so that a steady-state foam was established. The liquid hold-up ϵ evidently defined as the volume fraction of liquid in the foam, was found to become smaller as distance from the foam-liquid interface increased and was found to depend on superficial gas velocity, liquid viscosity, and surface viscosity. The value of rapidly approached an asymptotic value at distances greater than approximately 2 cm from the liquid-foam interface. The asymptotic value depended on the gas velocity and the liquid properties. Typical results are shown in Fig. 7. A mathematical model was developed to predict liquid hold-up profiles in the steady-state, semi-batch foams. A unique feature of the model is that the liquid flow rates at the foam-liquid interface required for solving the differential equations were calculated geometrically. It was shown that the results of the modelling calculations are not very sensitive to the boundary conditions, so that the geometrical method for estimating the boundary conditions is as effective as imposing experimental values. The results of the modelling calculations indicate that the model predicts the

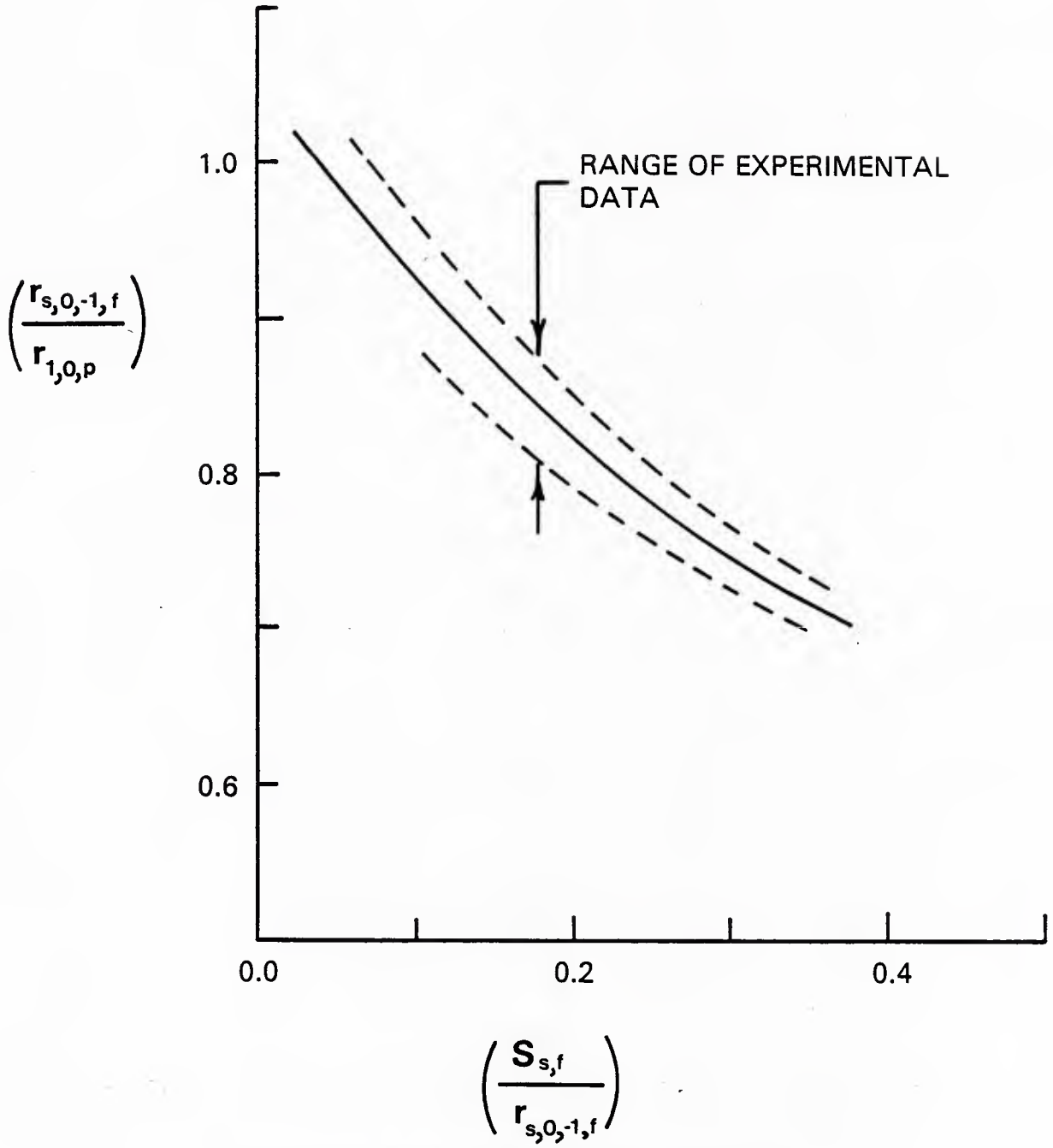

Fig. 5 — Ratio of measured mean bubble radius to true mean bubble radius for a newly-formed foam

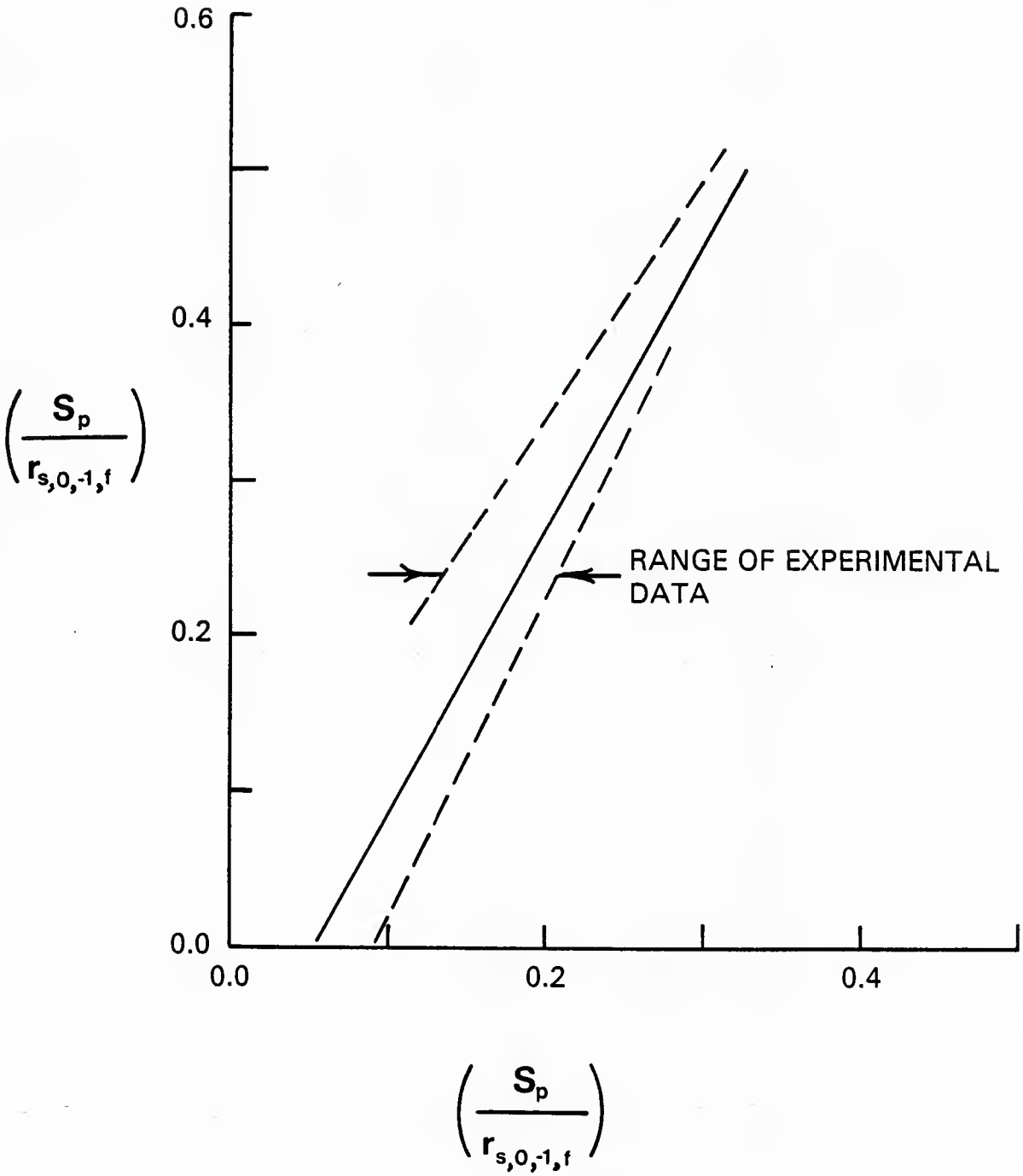

Fig. 6 — Relationship between true and measured standard deviations for a newly-formed foam

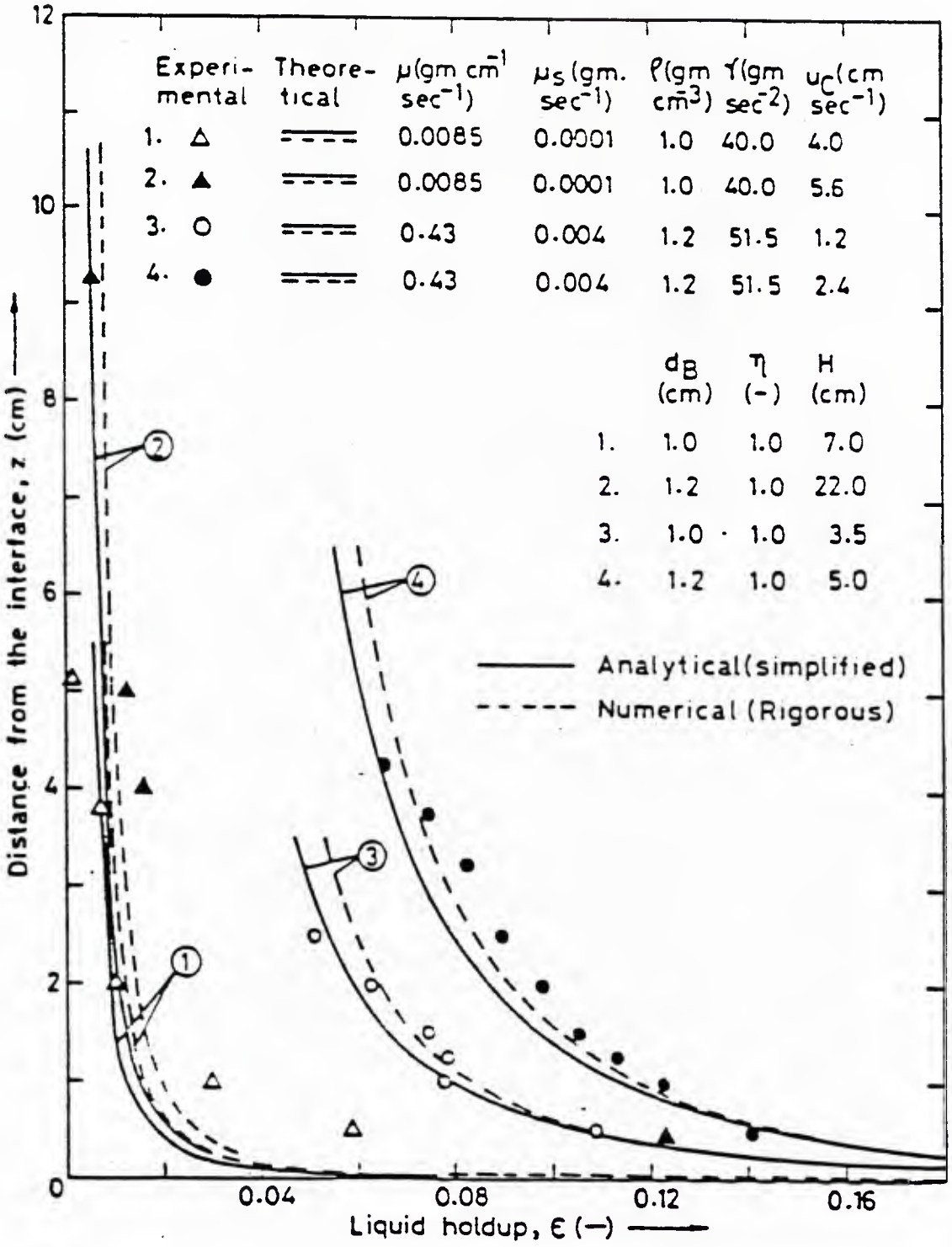

Fig. 7 — Effect of superficial gas velocity u_c and liquid viscosity on liquid hold-up ϵ

liquid hold-up profiles for water quite well, especially near the foam-liquid interface. For higher viscosity liquids, the predictions are not as good.

Davies and Rideal (1963) describe some simple methods for describing foams and foam properties, such as

$$\text{Expansion} = \frac{V_2}{V_1} \tag{15}$$

where V_2 = volume of the foam;
V_1 = original liquid volume.

The foam density, ρ, can be related to the liquid density, ρ_L, by

$$\rho = \rho_L \frac{V_1}{V_2}. \tag{16}$$

The foam viscosity can be up to 100 μ_L as measured in a viscometric flow device, because the bubbles must be deformed, because surface tension effects and surface viscosity are important, and because the films separating the bubbles must be detached from solid surfaces as the foam flows through the viscometer.

Princen (1983) presents an extensive discussion of foam rheology and develops a model relating shear stress and shear rate for an idealized foam composed of infinitely long cylindrical bubbles. This model incorporates elastic deformation up to a yield stress. For stresses greater than the yield stress, the foam flows, and an apparent viscosity can be calculated. The model is similar to the non-Newtonian Bingham plastic model sometimes used to describe the rheology of pastes and suspensions of solids. The yield stress and the shear modulus are directly proportional to the interfacial tension and inversely proportional to the bubble radius for monodispersed foams. The yield stress is a strong function of the volume fraction of gas, and the shear modulus is proportional to the square root of the volume fraction. The model was first developed for zero film thickness and zero contact angle. Then the model was extended to cover the more realistic cases of non-zero film thickness and contact angle. In most cases, as the contact angle increases, yield stress increases and the shear modulus decreases. Yield stress and shear modulus are higher for non-zero film thickness than for zero film thickness.

An approximate measure of the foam-forming characteristics of any particular liquid, the "foaminess," can be determined using a transparent tube fitted at the bottom with a porous septum. Gas is blown upward through the septum and through the liquid placed above the septum. The steady-state volume of foam formed is measured at constant volumetric gas flow rates. The foaminess is defined by

$$\Sigma = \frac{V_2}{u} \tag{17}$$

where V_2 = steady-state foam volume;
u = volumetric gas flow rate;
Σ = foaminess.

Typical values for Σ are on the order of 5 (clean seawater) to 3600 (surfactant solutions) seconds depending on the liquid properties.

The stability of a foam is a property which is of interest in many applications. A characteristic lifetime for a foam can be defined by

$$t_f = \frac{1}{V_2} \int V(t)\, dt \tag{18}$$

where V_2 = initial foam volume;
$V(t)$ = foam volume at any time after formation.

The volume of the foam changes with time, because liquid drains from the lamellae, and the bubbles break and coalesce due to mechanical shocks or vibrations induced by flow or surface tension effects.

Haas and Johnson (1968) have developed a mathematical model for the drainage of liquid in a stable foam, i.e. one for which the bubble size distribution is not changing. The liquid flows from the films separating the bubbles into the plateau border regions and then through the borders to the foam-liquid interface below the foam. In the films, the flow is driven by surface tension forces. In the plateau borders, the flow is driven by gravity. The mathematical model is based on liquid phase mass balances for the foam phase. For a stationary foam

$$\frac{\epsilon^2}{L_0 N} = \frac{32\mu}{\pi g} \frac{\pi k^2}{4}, \tag{19}$$

where ϵ = volume fraction of liquid in the foam;
L_0 = superficial liquid velocity for a stationary foam;
$N(1 - \epsilon)$ = number of plateau borders per unit cross-sectional area;
k = ϵ/ϵ_{PB} ;
ϵ_{PB} = fractional cross-sectional area for liquid flow in plateau borders.

The governing equation for flow in the foam is

$$\frac{\partial \epsilon}{\partial t} = \frac{\partial L_0}{\partial z}, \tag{20}$$

the position coordinate z is measured vertically upward. When Eqs. (19) and (20) are combined to eliminate L_0, the resulting differential equation can be solved by the method of separation of variables to give $\epsilon(t,z) = T(t)Z(z)$. The solution is

$$\epsilon(t,z) = \frac{\epsilon(t_0,z_0) - \frac{1}{2} c\, T_0 \left[\frac{32M}{\pi g}\right] \left[\frac{\pi N k^2}{4}\right] (z - z_0)}{cT_0(t - t_0) + 1}, \tag{21}$$

where c = integration constant;
T_0 = $T(t_0)$;
t_0 = initial value of time;
z_0 = reference position.

Equation (21) can be combined with Eq. (19) to determine L_0. The total amount of liquid drained from the foam in the time interval $(t - t_0)$ at any position z is

$$W(t,z) = \int_{t_0}^{t} L_0 dt. \tag{22}$$

At $z = z_0$, the equations can be simplified to give

$$W(t,z_0) = L_0(t_0,z_0) \frac{t - t_0}{cT_0(t - t_0) + 1}, \tag{23}$$

or

$$W(t,z_0) = \frac{\rho g}{32M} \frac{4}{\pi N k^2} \epsilon^2 t(t_0,z_0) \frac{t - t_0}{cT_0(t - t_0) + 1}. \tag{24}$$

The quantity cT_0 is evaluated in terms of the height of the column of foam, ℓ, and the superficial liquid velocity, $L(t_0,z_0)$, as

$$cT_0 = \frac{\rho g}{32M} \frac{4}{\pi N k^2} \frac{4}{\ell^2} L(t_0,z_0)^{1/2}. \tag{25}$$

The parameters ℓ and $L(t_0,z_0)$ must be determined experimentally. The value of N is related to the mean bubble diameter by $N \cong 2.5d^{-2}$. The experimental data reported by Haas and Johnson indicate that the model gives a good description of the drainage of liquid from a foam.

The foregoing development shows that the time interval over which a foam persists depends on the viscosity of the liquid. DeVries (1972) reports lifetimes of 15 minutes for a foam formed from a liquid having a viscosity $\mu_l = 0.5$ poise but lifetimes of "only a few minutes" for foams formed from water ($\mu_L = 0.01$ poise). In each case, $V_G/V_L = 10$. As a foam ages, the bubble size distribution changes, and this affects the foam stability. There are mechanisms which cause changes in bubble size distribution—gas diffusion between bubbles and bubble wall rupture and coalescence. The pressure difference between small and large bubbles is given by Eq. (2). This means that there is gas transport through the bubble wall from the small bubble to the large one. Eventually, the small bubble disappears. The rate of the gas transport is

$$\frac{dn}{dt} = PA_{12}\Delta p_{12} \tag{26}$$

where P = permeability of the bubble wall;
A_{12} = area of the bubble wall;
$\Delta p_{12} = 2\gamma \left[\frac{1}{r} - \frac{1}{R}\right]$;

r = radius of the small bubble;
R = radius of the large bubble;
n = moles of gas transferred.

The permeability can be calculated as

$$P = \frac{DS}{\left[\theta + \frac{2D}{k_1}\right]}, \tag{27}$$

where D = diffusion coefficient of the gas in the liquid;
S = solubility of the gas in the liquid;
θ = bubble wall thickness;
k_1 = mass transfer coefficient at the gas-liquid interface

defined by

$$\frac{dn}{dt} = k_1 A_{12}(C_0 - C); \tag{28}$$

C_0 = equilibrium concentration at the interface;
C = concentration in the gas phase.

There are two limiting cases,

$$P = \frac{DS}{\theta} \text{ if } \frac{2D}{k_1} << \theta \tag{29}$$

which applies if θ 10^{-4} cm, and

$$P = \frac{1}{2}k_1 S \text{ if } \frac{2D}{k_1} >> \theta. \tag{30}$$

For soap films, $\theta = 4 \times 10^{-7}$ cm, so that values of k, determined from flux measurements for soap films using the assumption of Eq. (18) show that $\frac{2D}{k_1} = 2 \times 10^{-6}$ cm.

Diffusion rate information can be related to bubble size distributions. Let A_{12} be approximately the area of the small bubble. The *excess* pressure in the small bubble then is approximately

$$\Delta p_{12} = \frac{2\gamma}{r}. \tag{31}$$

Combining Eqs. (26), (27), and (31) with the ideal gas law shows that the rate of shrinkage of a small bubble depends approximately on its own radius,

$$-r \frac{dr}{dt} = 2\gamma P \left[\frac{RT}{P_a}\right], \tag{32}$$

where R = gas law constant;
T = absolute temperature;
P_a = absolute pressure.

Integrating to obtain an equation for $r(t)$,

$$r^2(0) - r^2(t) = r_0^2 - r^2 = \frac{4RT}{P_a}\gamma Pt. \tag{33}$$

This shows that the bubble surface area decreases as a linear function of time. The bubble lifetime is calculated at $r = 0$, as

$$t(r_0) = \left[\frac{4RT\gamma}{P_a}\right]^{-1} r_0^2. \tag{34}$$

DeVries (1972) reports that for one case, $\frac{d}{dt}(r^2) \neq f(r_0)$. This implies that θ = constant and that P = constant. For another case, slight variations in $\frac{d}{dt}(r^2)$ with r_0 were found. This could have been due to variations in θ or P. If the permeability P, is constant for a particular foam, the change in size distribution frequency function $F(r_0)$, can be calculated after selecting a method for describing the distribution of permeated gas among larger bubbles. For example, the gas might be distributed among the larger bubbles in proportion to their surface areas.

The number density for bubbles is related to the initial number density, N_0, by

$$N_t = N_0(1 - \int_0^{r_{0,t}} F(r_0)\, dr_0) \tag{35}$$

where $F(r_0)$ = frequency distribution function at $t = 0$;
$r_{0,t}$ = initial radius of a bubble with lifetime t;
N_{dt} = number density at time t.

If $F(r_0)$ is known, then $N(t)$ can be calculated exactly knowing $r_0(t)$ from Eq. (36). For a particular foam formed mechanically in a high speed mixer, DeVries (1958) found that

$$F(r_0) = \frac{6\alpha\, r_0}{(1 + \alpha\, r_0^2)^4}, \tag{36}$$

where α is an adjustable parameter. This, together with Eqs. (34) and (35) gives the result

$$N_t = N_0\left[\frac{1}{1 + k_d t}\right], k_d = \left[\frac{4RT}{P_a}\right]\gamma\, P\, \alpha \tag{37}$$

where k_d is in the range $10^{-3} < k_d < 3.3 \times 10^{-3}$ seconds.

Bubble wall rupture and subsequent coalescence causes a spontaneous decrease in surface area in the foam as time goes on. Wall rupture depends on wall thickness and on the probability of rupture. Thin films are more likely to rupture than thick ones. Bubble wall lifetime is determined by the rate of thinning and the probability of rupture. For a bubble wall stabilized by rigid monolayers, flow patterns are relatively simple and thinning is relatively slow, where the

$$\text{(Rate of thinning)} \sim \frac{\theta^2}{\mu_L}.$$

For a mobile bubble wall, thinning is irregular. Thin spots form if the wall is relatively persistent. If the wall is very unstable, it thins and collapses rapidly after reaching a critical thickness of about 10^{-5} cm. In such a case

$$\text{(Bubble wall lifetime)} \sim \text{(Rate of thinning)} \sim \mu_L.$$

Bubble wall rupture can be initiated by the formation of a hole. Surface energy is converted to kinetic energy at the growing hole rim. The velocity of hole rim propagation is

$$u_r = \frac{2\gamma}{\sqrt{\theta\rho}} = \text{constant} \tag{38}$$

For $\theta = 10^{-4}$ cm, $u_r = 10^3$ cm/s. This means that rupture occurs only milliseconds after initiation or hole formation. Thus, initiation is the rate determining step for rupture. Hole formation is apparently necessary for rupture to occur. DeVries (1972) gives a discussion of possible causes for hole formation. One possible cause is that van der Waals forces cause fluctuations in film thickness to propagate. These thickness fluctuations are caused by thermal stresses or by some other mechanism. The thickness fluctuations grow spontaneously when the wavelength of the fluctuation, λ, is greater than some critical value. That is,

$$\lambda > \lambda_{crit} = \left[-\frac{2\pi^2\gamma}{\frac{d^2G}{d\theta^2}} \right]^{1/2}, \tag{39}$$

where G is the total free energy of interaction per unit surface area. Thickness fluctuations having $\lambda < \lambda_{crit}$ are damped.

Nishioka et al. (1983) measured foam stability by observing the pressure in the head space above a foam. The rate of increase of pressure was related to the decrease in surface area. They studied foams which had different drainage characteristics. They compared their measurements with calculations made using the mathematical model of Lemlich (1978). Typical results are shown in Fig. 8 The parameter K is a measure of permeability of the liquid films. Permeability increases as K becomes larger.

Djabbarah and Wasan (1985) studied the relationship between surface viscosity and foam stability. They measured the rupture time and found that rupture time increased as surface viscosity increased. The surface viscosity was modified by using surfactant solutions containing differemt concentrations of sodium lauryl sulfate and lauryl alcohol.

There are other forces acting on the bubble walls which can affect their stability. Forces associated with an electrical double-layer, viscoelastic forces, and forces associated with surface tension gradients all have an effect. There also may be time varying concentrations of surfactants absorbed on the bubble wall. Such gradients in surfactant concentration can cause surface tension gradients which can either increase or decrease stability. If the surface tension is lower at a point on the wall than it is at surrounding points, surface energy can be increased by extension of the area of lower surface tension and contraction of the area of higher surface tension. This can lead to rupture if the rate of thinning is higher than the rate of decrease of the surface tension gradient. The surface tension gradient would normally be reduced by surface diffusion of the surfactant. If this diffusion is too slow to restore equilibrium, then local thinning of the bubble wall can lead to rupture.

AIR ENTRAINMENT

As was mentioned earlier, agitation is one method for mixing air into a liquid. The turbulent flow in a breaking wave is one type of strong agitation suitable for foam formation. This has been discussed by Longuet-Higgins and Turner (1974) who developed a heuristic mathematical description of a "spilling" breaker. They calculated approximate crest-region shapes and discussed how the length of the whitecap on the breaker is related to the energy balance in the wave. The rate of air entrainment at the base of the whitecap is a topic left for future work. More recently Griffin (1984) has discussed the overall aspects of wave breaking, including the formation of white water and foam.

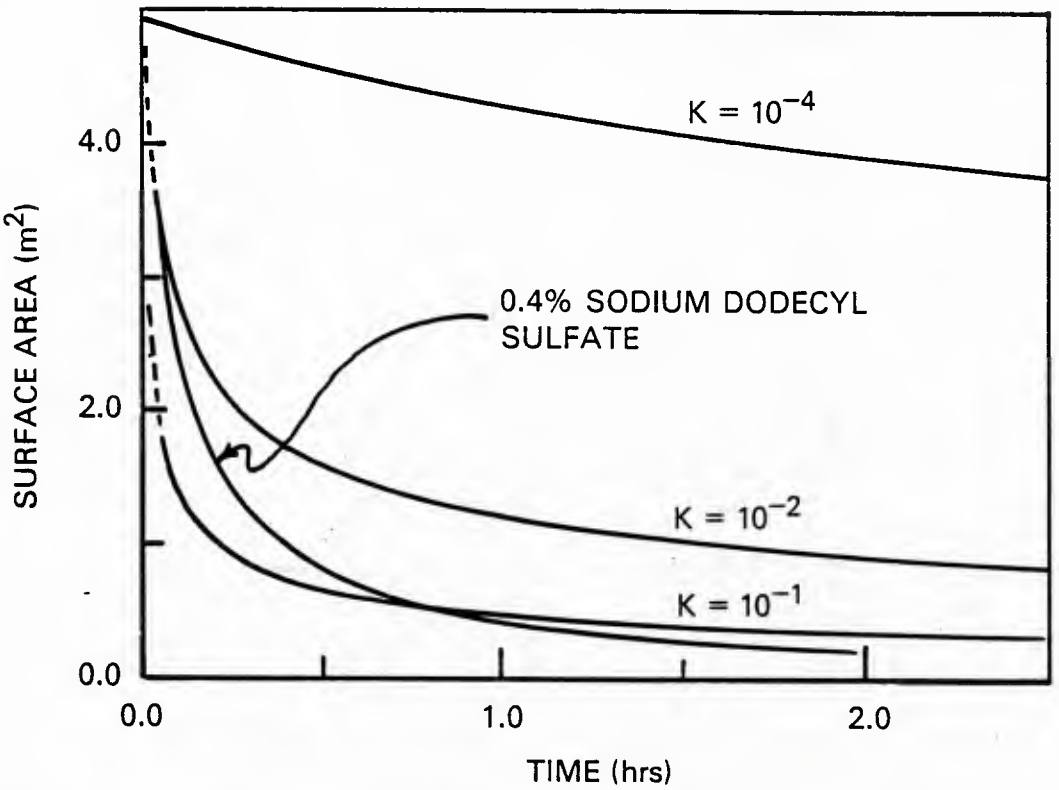

Fig. 8 — The experimental decay of a 0.4% sodium dodecyl sulfate foam compared with computed decays. The value K = 10^{-4} cm^2/hr represents the theoretical decay of a nondraining system.

Examples of the air entrainment and formation of bubbles during the breaking of steep surface waves are given by Su, Green and Bergin (1984). A typical example of a spilling breaker is given in Fig. 9. The region of white water containing entrained air is clearly visible.

Mixing air and water by means of plunging jets and by the action of turbulent eddies in water flowing over spillways has been discussed by several authors. Data for the entrained air flow rate are presented by Van De Sande and Smith (1972, 1973, 1976). They directed a jet of water at the surface of a pool of water at such an angle that the entrained air was carried into a collection chamber connected to a vacuum system. The entrained air flow rate was measured directly, and the data were presented in terms of the ratio of the flow rate, α_j, to the jet flow rate, ϕ_j. Their experimental results can be summarized as follows. For low velocity jets for which the jet velocity, V_j, is in the range 2m/sec $< V_j <$ 5m/sec, there are two relationships, depending on the length of the jet. These are:

$$\text{Short jets: } L_j < 0.9\, L_B, \text{ where } L_B = 320 D_n^{1.5} V_j,$$

$$\frac{\phi_A}{\phi_j} = \frac{0.027 V_j}{\sin \alpha} \frac{V_j^{1/3}}{D_j^{1/2}} \quad \text{(SI units).} \tag{40}$$

Long jets: $L_j > 0.9\, L_B$,

$$\frac{\phi_A}{\phi_j} = \frac{8.5 \times 10^{-6}}{\phi_j} + (1.05 \times 10^{-4})\, \rho_w V_j^2 \quad \text{(SI units)} \tag{41}$$

where L_j = jet length;
L_B = jet length at break-up;
D_j = jet diameter;
α = angle between jet and the liquid surface;
ρ_w = density of the water;
D_n = nozzle diameter.

For high velocity water jets for which

$$V_j > \left[\frac{10\, \gamma}{\rho_A D_n} \right]^{1/2} \tag{42}$$

where γ = surface tension,
ρ_A = density of air,
the results are presented in graphical form (see Fig. 2 in the 1973 paper by Van De Sande and Smith). These results are sketched in Fig. 10. The jet diameter is related to the nozzle diameter by

$$\frac{D_n}{D_j} = 0.085 \left[\left(\frac{\rho_A V_j^2 D_n}{\gamma} \right) \left(\frac{\rho_w V_j D_n}{\mu_w} \right) \right]^{1/6} = 0.085 \left[N_{We}\, N_{\mathrm{Re}} \right]^{1/6} \tag{43}$$

for $N_{We} N_{\mathrm{Re}} > 7 \times 10^6$.

Fig. 9 — A laboratory photograph of a deep water spilling breaker;
from Ramberg and Griffin (1987)

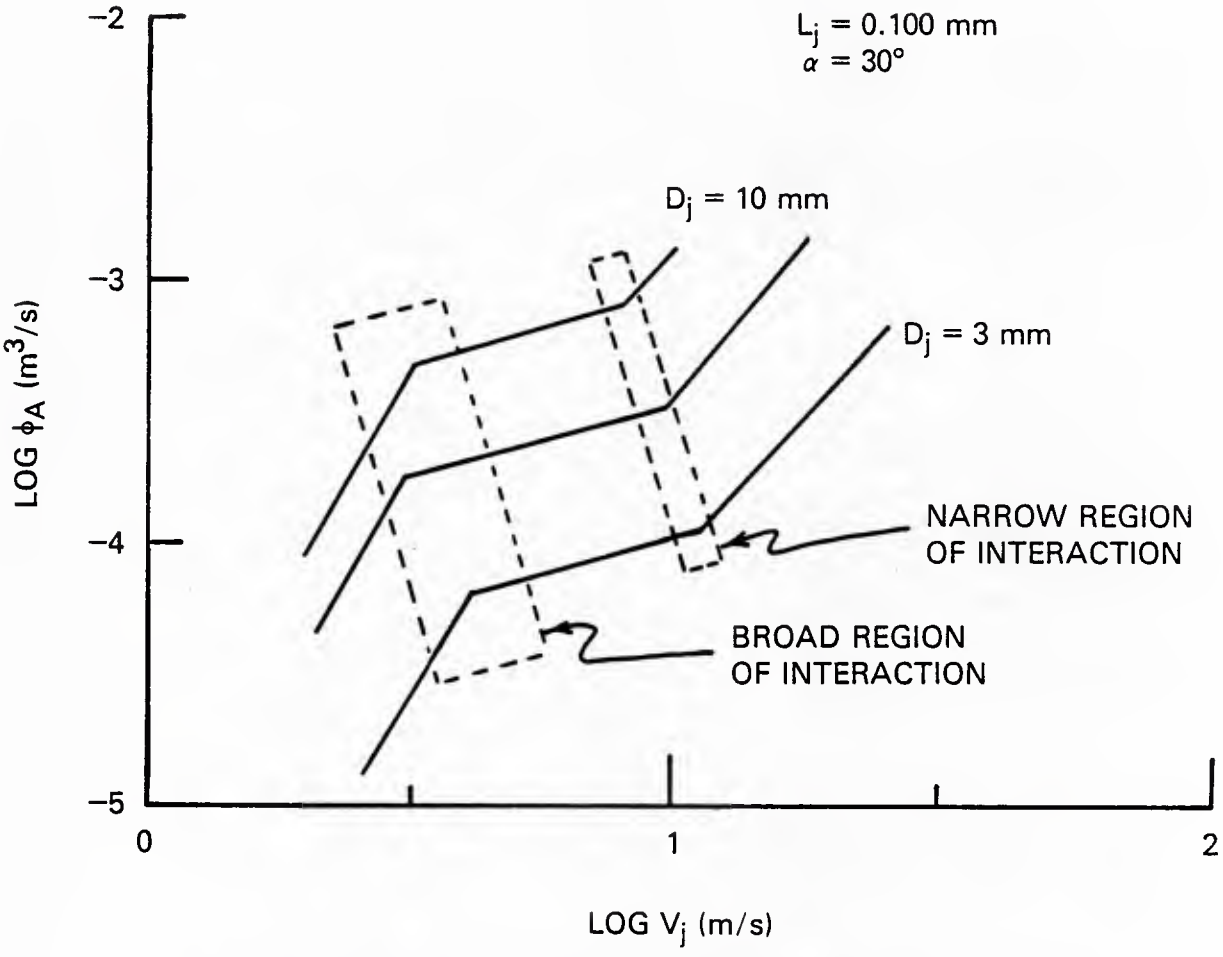

Fig. 10 — Air entrainment by high velocity jets; from Van De Sande and Smith (1973)

The effect of the angle of impact on the air entrainment rate is

$$\phi_A (\sin \alpha)^{1/4} = \text{constant.}$$

The mechanism for entrainment is described in the 1972 paper by Van De Sande and Smith. Cavities are formed by droplet or jet impact, and bubbles are enclosed. A rough-surfaced jet entrains more air than a jet having a smooth surface. Burgess, Molloy and McCarthy (1972) discuss the surface roughness of a jet and relate the roughness to the amount of air entrained. Thus,

$$\frac{\phi_A}{\phi_j} = \left[\frac{D^*}{D_n}\right]^2 - 1 \tag{44}$$

where D^* is the diameter of the envelope which encloses all the roughness elements of the jet. The diameter D^* depends on L_j, the length of the jet, since the jet expands as it moves away from the nozzle. Burgess et al. also show how the interfacial area of bubbles entrained is related to the jet velocity and surface roughness. These data were determined by CO_2 entrainment and subsequent reaction with sodium hydroxide solution. They calculated the interfacial area according to the equation

$$a = \frac{R_a}{C^* \sqrt{D k_2 b_0}} \tag{45}$$

where a = interfacial area per unit volume in the entrainment zone;
D = diffusion coefficient;
R_a = reaction rate;
C^* = equilibrium CO_2 concentration;
b_0 = NaOH concentration in the liquid;
k_2 = reaction rate constant;

and found that in SI units

$$a = (4.5 \times 10^{-3}) \left[\frac{D^*}{D_n}\right] V_j - (1.75 \times 10^{-2}). \tag{46}$$

The effects of jet surface roughness on gas entrainment are also discussed by McKeogh and Ervine (1981). They report the entrainment rate to be

$$\frac{\phi_A}{\phi_j} = 1.4 \left[\left[\frac{\epsilon}{r}\right]^2 + 2\left[\frac{\epsilon}{r}\right] - 0.1\right]^{0.6} \tag{47}$$

where ϵ = one-half jet surface roughness;
r = mean jet radius.

They determined the size of the region in the liquid which was affected by air entrainment and measured the concentration of air in that region. The concentration of air was expressed as

$$C = \frac{100 \times \text{Volume of air}}{\text{Volume of air} + \text{Volume of water}}.$$

The depth of penetration of the entrained air was

$$D_p = 2.6\,(V_j D_j)^{0.7}. \tag{48}$$

The center line air concentrations are given by

$$\frac{C_c}{C_{\max}} = \frac{1}{1 + 3\left[\frac{x}{D_p}\right]^3} \tag{49}$$

where x = distance below the surface.

The radial dependence of air concentration is given for two regions

$$\frac{C}{C_c} = \frac{1}{1 + 5\left[\frac{r}{r_x}\right]^2 - 10\left[\frac{r}{r_x}\right]^3}, x < \frac{D_p}{2} \tag{50}$$

$$\frac{C}{C_c} = 1 - \frac{r}{r_x}, x > \frac{D_p}{2} \tag{51}$$

where r_x = radial extent of the bubbly region.

Lara (1979) has discussed the conditions necessary for air to be entrained by a plunging jet. He finds that whether or not air entrainment occurs depends on the jet length to diameter ratio and on the jet velocity. His results are summarized in Fig. 11. The jet velocity is much lower than the jet velocities used in the other work discussed here.

Research on air entrainment in water flowing over a spillway has been reported by Gangadharaiah et al (1970), by Keller and Rastogi (1975), and by Wood (1983). Their work centers on mathematical modelling of the turbulent boundary layer along the spilling surface. They believe that air entrainment begins when the outer edge of the boundary layer coincides with the surface Their calculations agree with experimental results and observations made for full-size operating spillways. They report the position at which air entrainment begins as a function of flow rate. Gangadharaiah et al also report the concentration of air in aerated flow in a water channel, but they do not relate this to the turbulence characteristics of the flow.

Volkart (1982) studied air entrainment in a partly filled pipe and related his results to air entrainment in open channel flow. The mechanism suggested for the air entrainment is that turbulent impulses perpendicular to the surface cause water droplets to be ejected into the air. When these droplets fall back into the water, they entrain air. In order for water droplets to be ejected, the turbulent boundary layer must have reached the surface, and the turbulent impulse in the transverse direction must exceed a critical value. He postulates that this occurs somewhat farther downstream than the point at which the turbulent boundary layer just reaches the surface. Apparently, some extra distance is required for the turbulence intensity to reach the required value. The concentration of entrained air in water was measured using an electrical conductivity method based upon the difference between the conductivity of water and air. The mean air concentration was correlated by the equation

$$C = \frac{Q_a}{Q_a + Q_w} = 1.0 - \frac{1.0}{(0.02N_{BOU} - 6.0) + 1.0} \quad N_{BOU} \geq 6; \tag{52}$$

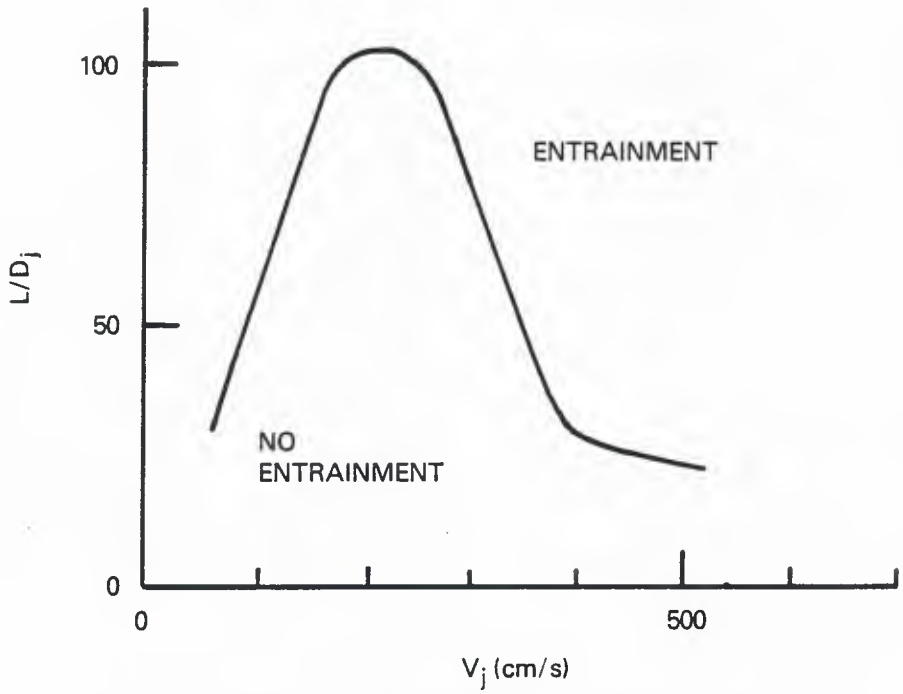

Fig. 11 — Conditions for air entrainment by jets; adapted from Lara (1979)

where Q_a = volumetric flow of air in the mixture;
Q_w = volumetric flow of water in the mixture;
N_{BOU} = Boussinesq number = $\dfrac{V_w}{\sqrt{gR_w}}$
V_w = water velocity with air bubble entrainment excluded;
R_w = mean hydraulic radius.

Equation (52) shows that air is entrained only if N_{BOU} 6. Volkart determined that there is a minimum slope for which $N_{BOU} = 6$ and for which air entrainment can be initiated. This slope is given by

$$J_A = \frac{9}{8}\left[\frac{1}{-\log\dfrac{2.51\nu}{D\sqrt{2gDJ_a}} + \dfrac{k_s}{3.71D}}\right]^2 ; \frac{H}{D} = 1.0 \tag{53}$$

where J_A = slope;
k_s = roughness height;
H = water depth.

The relationship giving friction losses for flow in rough pipes described by Colebrook (1938) was used here. For depth-to-diameter ratios different from 1.0, a correction factor is applied.

$$J_A = J_A\Big|_{\frac{H}{D}=1} f\left(\frac{H}{D}\right) \tag{54}$$

The correction factor $f(H/D)$ is obtained graphically. Typical values are

$$\frac{H}{D}: 1.0 \quad 0.9 \quad 0.8 \quad 0.6 \quad 0.5 \quad 0.4 \quad 0.35$$

$$f\left(\frac{H}{D}\right): 1.0 \quad 0.94 \quad 0.94 \quad 0.96 \quad 1.0 \quad 1.05 \quad 1.08.$$

The initiation of air entrainment depends on pipe diameter, roughness height, and depth to diameter ratio. The results that air entrainment begins at lower values of J_A for large smooth-walled pipes than for small rough-walled pipes. The author says this is evidence that turbulence is a more important factor than wall roughness when it comes to describing air entrainment. The critical velocity for air entrainment to occur is

$$V_{w,crit} = 6\sqrt{gR_w}. \tag{55}$$

The mean velocity of the entire air-water mixture was found to be smaller than the mean velocity for the water only, or

$$\frac{V_m}{V_w} = (1 - C^{2.09}). \tag{56}$$

The air concentrations for flow in partly filled pipes are smaller than those for open channel flow at the same conditions of slope, roughness height and depth to diameter ratio.

MARINE HYDRODYNAMICS APPLICATIONS

Wave Breaking There are many causes for the breaking of ocean waves. These include the relative motion between the water and, say, a ship in a seaway or a cylindrical obstacle in a wavefield; wind blowing over the water; superposition of and nonlinear interactions between wave components; concentration of wave energy by refraction; and the shoaling of waves. These various causes result in two predominant types of breaking waves: the plunging breaker, in which the wave crest curls forward and plunges into the slope of the wave at some distance away from the crest; and spilling breakers, in which the broken region tends to develop more gently from an instability at the crest and often forms a quasi-steady whitecap on the forward face of the wave. Foam and bubbles from the entrained air often play an important and visible role in the processes of spilling and plunging.

A third type, surging, sometimes develops as waves are incident upon a sloping beach. In this case, if the slope is very steep or the wave steepness is very small, the waves do not actually break but surge up and down to form a standing wave system with little or no air entrainment. A fourth case, collapsing, is considered to be a special limiting case of the plunging breaker. Collapsing occurs when the crest remains unbroken, but the lower part of the front face of the wave steepens and falls and then forms an irregular region of turbulent water. Galvin (1968) has provided a historical recently, the breaking of waves on beaches has been discussed in some detail by Peregrine (1983).

The breaking of waves, with particular emphasis on the processes which occur in deep water, also has been discussed by Griffin (1984). From numerous small-scale experiments it is generally expected that air entrainment is not a determining factor in understanding or predicting the dynamics of breakers (D.H. Peregrine, 1984; private communication). However, air entrainment and the ensuing formation of bubbles and foam do give a measure of the intensity and extent of the turbulence which is produced by spilling and plunging breakers. Two examples are shown in Figs. 12 and 13. A laboratory simulation of the air entrainment and bubble formation processes during wave breaking is shown in Fig. 12. The formation of a bubble cloud beneath the breaker is clearly visible, and it is evident that even this nominally simple laboratory-scale flow is very complex. The breaking of a steady surface wave and the ensuing formation downstream of a turbulent white water wake region is shown in Fig. 13. The wave train was generated by towing a foil-shaped body beneath the free surface. Again the flow field is very complex for even this simple configuration. Further progress toward modeling and understanding the turbulent regions of foam and bubbles in breaking waves is likely to be empirical for some time to come, except for simple models of bubble clouds as described in the next section.

The extent of surface coverage by foam and bubbles is important in characterizing and interpreting the return from remote sensing devices such as microwave radiometers and microwave radars which are deployed above the sea surface. The radiation from the ocean surface that is measured by microwave radiometry is a sum of the thermal emission of the water and the reflection of the sky's radiation from the sea surface. Foam greatly increases the microwave emissivity of the water surface (Droppleman, 1970; Stogryn, 1972; Koepke, 1986) by altering the reflectivity (emissivity = 1 - reflectivity) due to absorption and reflection from the upper air-foam and the lower foam-water interfaces. The foam-induced increase in emissivity is primarily responsible for the large increase in the microwave brightness temperature of the sea.

The presence of surface foam can contribute significant backscatter to microwave sensors (Alpers, Ross and Rufenach, 1981; Keller, Plant and Valenzuela, 1986). In addition to the return from pure Bragg scattering, there are contributions from specular scattering by the wave/turbulent fluid interfaces normal to the incidence angle of the radar and volume scattering when the foam is

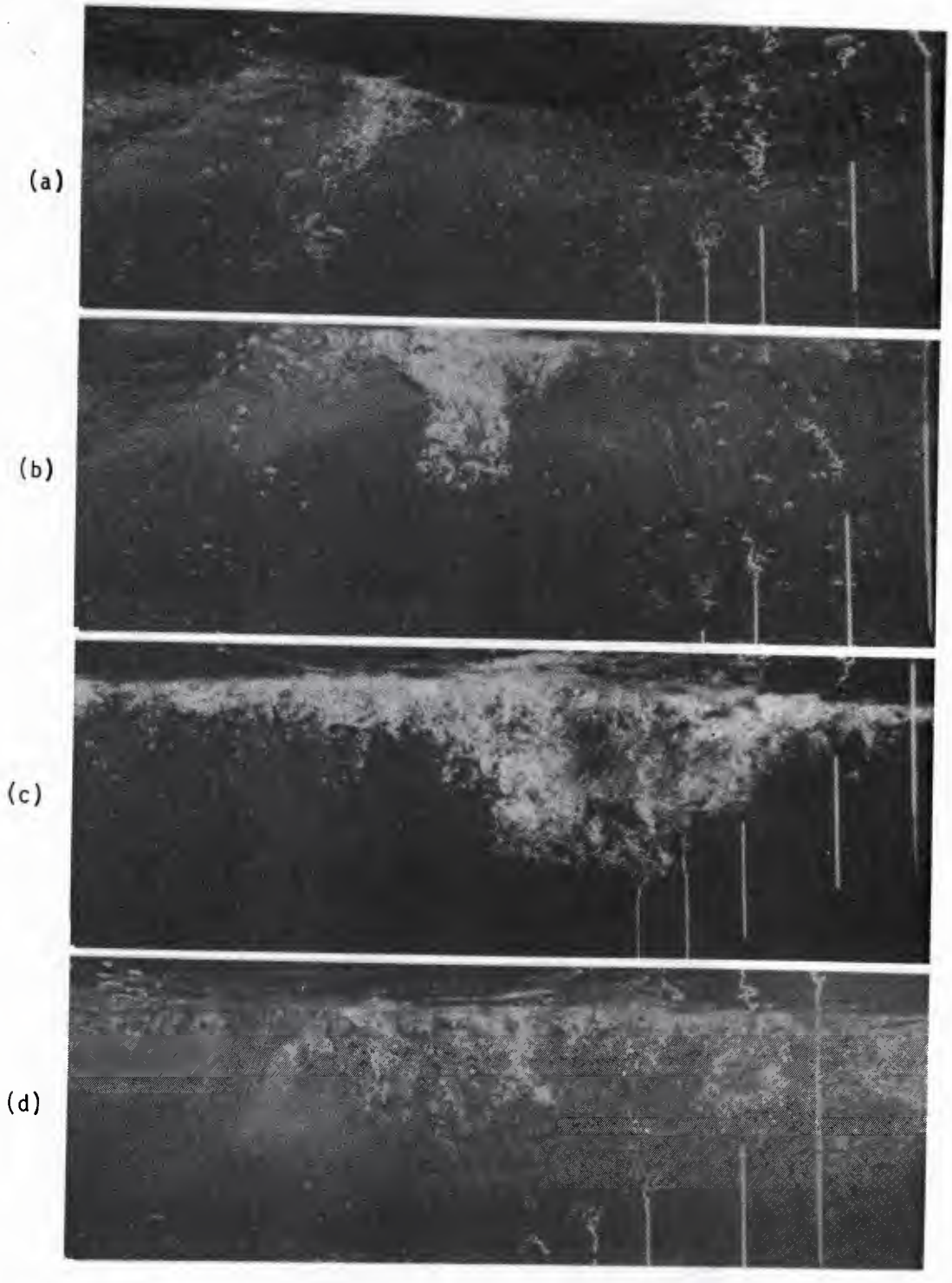

Fig. 12 — Sequence of air entrainment and bubble formation in a breaking wave. The wave moves from left to right; from Su, Green and Bergin (1984).

Fig. 13 — A steady breaking surface wave and the ensuing turbulent wake downsteam from a submerged, towed hydrofoil. Photo courtesy of J.H. Duncan.

well aerated. Significant penetration of the radiation into the foam takes place when the dielectric properties of the foam approach those of air. More aspects related to whitecaps and white water generation by breaking surface waves are discussed in the proceedings of a recent whitecap workshop (Monahan and MacNiocall, 1986).

Surface Ship Wakes. Figure 14 illustrates the major sources of surface foam and bubble production from displacement-type vessels and defines some of the relevant terminology. The surface wake can be divided into three regions. These are the near wake, the far wake, and the Kelvin wave system.

The Kelvin wave system 19.5 boundary (cusp lines) and 35.3 cusp-crest tangent lines are illustrated in the figure. The apex of the boundary lines is located about one ship length ahead of the bow (Newman, 1970). The transverse and divergent wave crests are visible for many ship lengths astern and to either side of the ship's path. Surface foam and bubbles can be produced when the divergent waves in the Kelvin wave system break at wave steepnesses ak, where a is the wave amplitude and $k = 2\pi/L$ is the wavenumber, greater than $ak \simeq 0.34$ (Ramberg and Griffin, 1987). Energy input into the Kelvin wave system by a vessel's movement throught the water and/or the interaction of the Kelvin wave and ambient wave fields also can cause the wave steepness to exceed $ak = 0.34$. Figure 1 shows breaking (spilling type) divergent waves almost directly perpendicular to the midsection on the port and starboard sides of the ship.

There are three major sources of foam and bubble production in the near wake region. The bow wave that is generated by the ship's motion will break if its steepness is greater than about $ak = 0.34$. The turbulent region adjacent to the ship's hull produces foam and bubbles because of the frictional drag forces on the surface of the hull. The initial spreading region (ISR) of the propeller wake is a region of high angular divergence of foamy water directly aft of the ship's stern. It is generally outlined by what appears to be a spilling-type breaking wave.

At greater distances downstream in the far wake, the surface foam and bubbles decay. The persistence of the foam depends on the time it takes for the bubbles to break after they reach the surface. The major factors that increase the stability of a bubble at the surface are increasing salinity (Miyake and Abe, 1948; Peltzer and Griffin, 1987; Monahan and Zeitlow, 1969; Scott, 1975), decreasing water temperature (Miyake and Abe, 1948) increased surface viscosity (Kitchener and Cooper, 1959), and the presence of organic surface-active materials which reduce the surface tension and modify the surface rheology (Adamson, 1976; Akers, 1976; Bikerman, 1973). A recent photographic analysis (Peltzer, 1984) revealed that the length of this foamy white-water region (Lww) can be described equally well by the equations

$$L_{ww} = 65.5\, V_s^{1.5} n^{-0.5}$$

and $$L_{ww}/L_{wL} = 53.5\, [V_s/(gL_{wL})^{0.5}]^{1.40}$$

where V_s (m/s) is the ship speed, L_{wL} is the waterline length (m), n is the propeller revolutions per second and g is the gravitational constant (m/s^2).

A typical wake profile taken of a surface vessel at ultrasonic frequency is shown in Fig. 15, which has been adapted from a Naval Ocean Systems Center (NOSC) study. The wake begins at the propellor and then increases to a depth of two to three times the ship's draft. According to the study, the rapid wake depth increase is accompanied by very high bubble density during the first 10 to 20 seconds. This probably represents the initial spreading region of the wake. It should be noted that the wake width increase at these early times is much more rapid than the estimate given in the figure. The bubble density decreases at times between 20 and 200 seconds, the wake depth remains relatively

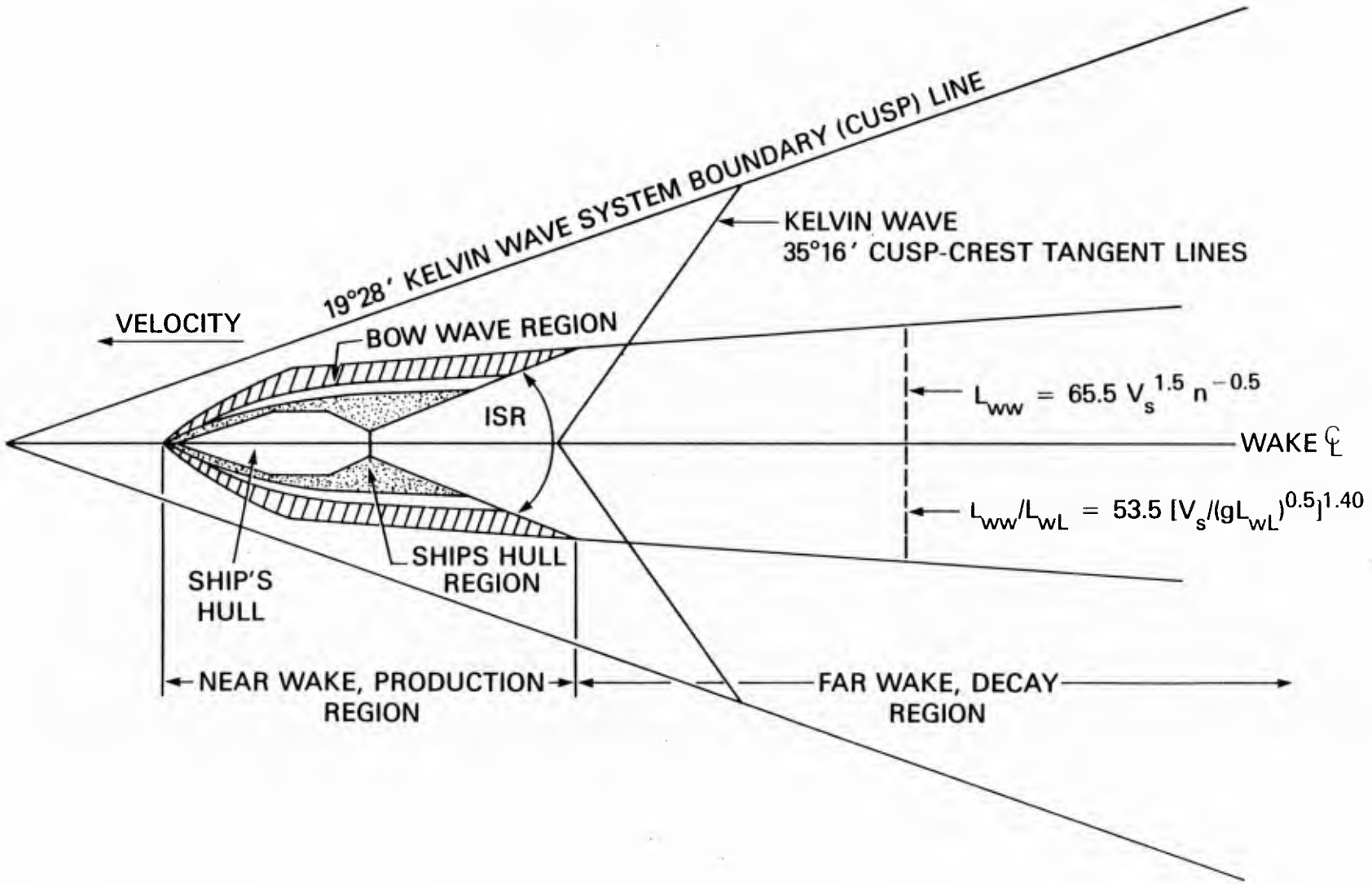

Fig. 14 — Three major sources of white-water production from displacement vessels; from Peltzer (1984)

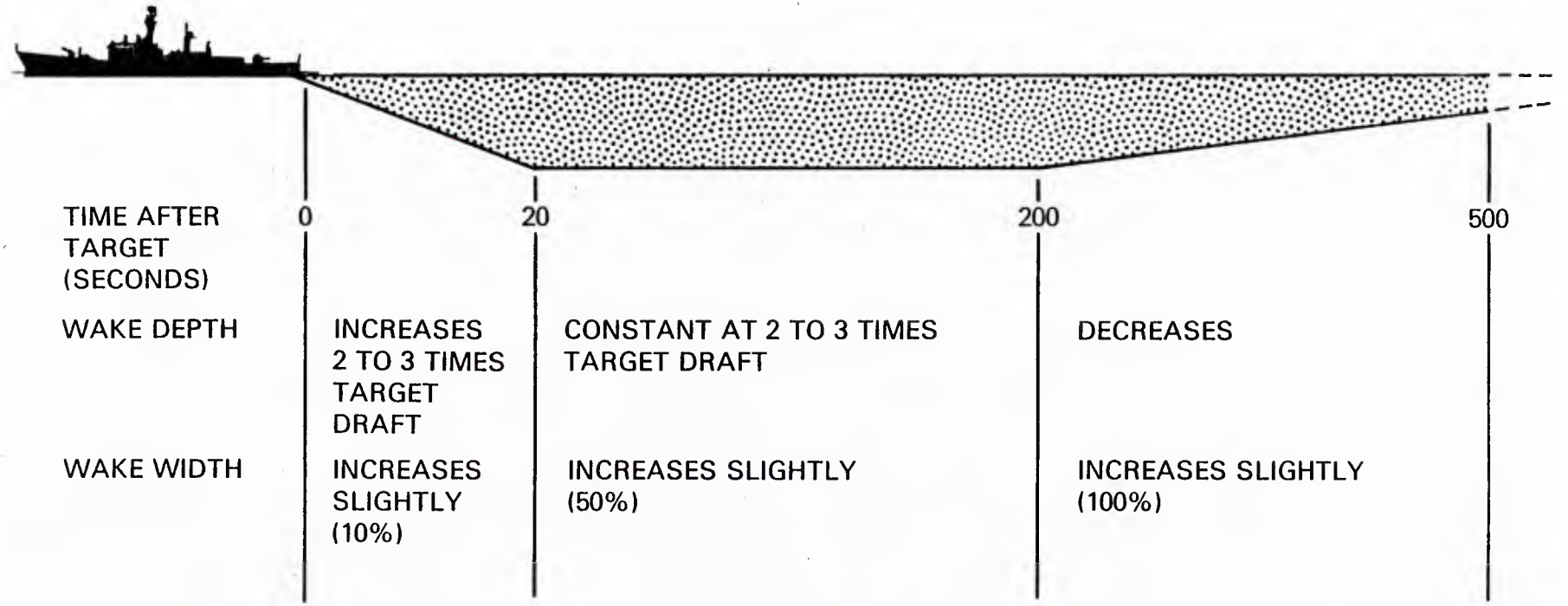

Fig. 15 — A general surface wake profile measured acoustically at ultrasonic frequency

constant at two to three times the ship's draft, and the wake width is somewhat greater than the ship's beam. At times beyond 200 seconds the depth of the wake gradually decreases and the wake width spreads to about twice the ship's beam. The time period between 20 and 500 seconds probably represents the far wake. For a typical 125 m long ship moving at 5.2 m/s, a time of 500 seconds represents a downstream distance of 11 ship lengths.

Modelling of the downstream surface ship wake will depend on the availability of appropriate initial conditions. One logical place to specify these conditions is in a vertical plane at the end of the initial spreading region. Then the spatial and temporal evolution of the far wake region, in principle, can be computed. However, the computations are strongly dependent on good initial conditions which in turn depend upon the accurate characterization of the several sources of foam and bubble generation upstream of the far wake.

The residence time of a single or multilayer foam at the surface and the bubbles in the underlying water column depends on the stability of the bubbles in those layers. Some of the major factors that influence the stability of bubbles include the water temperature, the air-sea temperature difference, the surface viscosity, the presence of organic surface-active materials, water cleanliness, and the presence of biological organisms and particulate matter. Other important factors include the salt content or salinity of the water, the size of the bubbles, the humidity and velocity of the air above the foam layer and the thickness of the liquid lamallae. All of these factors must be considered when the initial conditions are specified.

It will be necessary further to specify the relative proportions of foam and the "normal" two-phase mixture of bubbles and sea water. The foamy region is confined to a relatively thin vertical layer just at and below the surface. This is a highly agitated and aerated region with a high relative content of air to water. It may be possible to assume that the foam density is constant in the region. Then below this is the bubble wake which extends vertically downward over a greater distance. The sparse knowledge which is available concerning the vertical distance over which the wake extends is summarized in Fig. 15. Typically, acoustic measurements of the vertical wake thickness have dealt primarily with the bubbly region. As noted previously the thickness of this region is approximately two ship drafts in depth. The vertical extent of the overall turbulent ship wake probably is greater still. Models such as the ones described by Thorpe (1982) and Miner et al (1986) for the motions of individual bubbles and clouds of bubbles in seawater may provide a first step toward a more complete understanding of the bubble-dominated portion of the turbulent wake.

ACKNOWLEDGEMENTS

This study was conducted as part of the research program in free surface hydrodynamics at the Naval Research Laboratory. The work was initiated while one of the authors (D.W.H.) held an ONR/ASEE Fellowship appointment at NRL.

REFERENCES

A.W. Adamson, 1976, *Physical Chemistry of Surfaces*, Third Edition, John Wiley and Sons: New York.

W.R. Alpers, D.B. Ross and C.L. Rufenach, 1981, "On the Detectability of Ocean Surface Waves by Real and Synthetic Aperture Radar," J. Geophys. Res., Vol. 86, No. C7, 6481.

J.J. Bikerman, 1973, *Foams*, Springer Verlag: New York.

J.J. Bikerman, 1965, *Chemistry and Physics of Interfaces*, S. Ross (ed.), Am. Chem. Society, Washington, D.C., pp. 58-61.

J.M. Burgess, N.A. Molloy and M.S. McCarthy, 1972, "A Note on the Plunging Liquid Jet Reactor," Chem. Engng. Sci., Vol. 27, 442.

H.C. Cheng and R. Lemlich, 1983, "Errors in the Measurement of Bubble Size Distribution in Foam," Ind. Eng. Chem. Fund., Vol. 22, 105.

C.F. Colebrook, 1938, "Turbulent Flow in Pipes," J. Inst. Civil Eng., Vol. 11, 133.

A.J. DeVries, 1972, "Morphology, Coalesence, and Size Distribution of Foam Bubbles," *Adsorptive Bubble Separation Techniques*, R. Lemlich (ed.), Academic Press: New York, 7-31.

A.J. DeVries, 1958, "Foam Stability III. Spontaneous Foam Destablization Resulting from Gas Diffusion," Rec. des Travaux Chimiques des Pays-Bas, Vol. 77, 283.

D. Desai and R. Kumar, 1983, "Liquid Hold-up in Semi-Batch Cellular Foams," Chem. Eng. Sci., Vol. 38, 1525.

J.T. Davies and E.K. Rideal, 1963, *Interfacial Phenomena*, Third Edition, Academic Press: New York, 393.

N.F. Djabbarah and D.T. Wasan, 1985, "Foam Stability: The Effect of Surface Rheological Properties on Lamella Rupture," AIChE Journal, Vol. 31, 1041.

J.D. Droppleman, 1970, "Apparent Microwave Emissivity of Sea Foam." J. Geophys. Res. Vol. 75, No. 3, 696.

T. Gangadharaiah, N.S. Lakshmana Rao and K. Seetharamiah, 1970, "Inception and Entrainment in Self-Aerated Flows," Proc. ASCE, Vol. 96 (HY7), 1549.

O.M. Griffin, June 1984, "The Breaking of Ocean Surface Waves," Naval Research Laboratory Memorandum Report 5337.

P.A. Haas and H.F. Johnson, 1968, "A Model and Experimental Results for Drainage of Solution Between Foam Bubbles," Ind. Eng. Chem. Fund., Vol. 6, 225.

R.J. Keller and A.K. Rostogi, 1975, "Prediction of Flow Development on Spillways," Proc. ASCE, Vol. 101 (HY9), 1171.

W.C. Keller, W.J. Plant and G.R. Valenzuela, 1986, "Observations of Breaking Ocean Waves with Coherent Microwave Radar," *Wave Dynamics and Radio Probing of the Ocean Surface*, Plenum Press, 285.

J.A. Kitchener and C.F. Cooper, 1959, "Current Concepts in the Theory of Foaming," Quar. Rev., Vol. 13, 71.

A.M. Kraynik, 1983, "Foam Drainage," Sandia Laboratories Report SAND83-0844.

R. Lemlich, (ed.) 1972, *Absorptive Bubble Separation Techniques*, Academic Press: New York, pp. 16-18.

R. Lemlich, 1978, "Prediction of Changes in Bubble Size Distribution Due to Interbubble Gas Diffusion in Foam," Ind. Eng. Chem. Fund., Vol. 17, 89.

P. Lara, 1979, "Onset of Air Entrainment for a Water Jet Impinging Vertically on a Water Surface," Chem. Eng. Sci., Vol. 34, 1164.

M.S. Longuet-Higgins and J.S. Turner, 1974, "Entraining Plume Model of a Spilling Breaker," J. Fluid Mech., Vol. 63, 1.

E.J. McKeogh and D.A. Ervine, 1981, "Air Entrainment Rate and Diffusion Pattern of Plunging Liquid Jets," Chem. Eng. Sci., Vol. 36, 1161.

E.W. Miner, O.M. Griffin and R.A. Skop, 1986, "Near-Surface Bubble Motions in Seawater," NRL Memorandum Report 5756.

Y. Miyake and T. Abe, 1948, "A Study on the Foaming of Sea Water, Part 1," J. Marine Res. Vol. 7, No. 2, 67.

E. C. Monaham and G. MacNiocaill (eds.), 1986, *Oceanic Whitecaps and their Role in Air-Sea Exchange Processes*, D. Reidel/Galway University Press.

National Defense Research Council, *Physics of Sound in the Sea*, NAVMAT Publication P-9675 (1969); a reprint of an earlier version compiled during and after World War Two.

J.N. Newman, 1970, "Recent Research on Ship Wakes," *Eighth Symposium on Naval Hydrodynamics: Hydrodynamics in the Ocean Environment*, Office of Naval Research, Dept. of the Navy, 519.

G.M. Nishioka, S. Ross and M. Whitworth, 1983, "The Stability of Foam: Comparison of Experimental Data and Computed Results, J. Coll. Interface Sci., Vol. 95, 435.

R.D. Peltzer, 1984, "White Water Wake Characteristics of Surface Vessels," NRL Memorandum Report 5335.

R.D. Peltzer, W.D. Garrett and P.M. Smith, 1987, "A Remote Sensing Study of a Surface Ship Wake," Int. J. Remote Sensing, Vol. 8, No. 5, 689.

R.D. Peltzer and O.M. Griffin, 1987, "Stability and Decay Properties of Foam in Seawater," NRL Memorandum Report 5949.

H.M. Princen, 1983, "Rheology of Foams and Highly Concentrated Emulsions," J. Coll. Interface Sci.,Vol. 91, 160.

S.E. Ramberg and O.M. Griffin, 1987, "Laboratory Studies of Steep and Breaking Deep Water Waves," Proc. ASCE, J. Waterways, Port, Coastal and Ocean Engineering, Vol. 113, No. 5, 493.

J.C. Scott, 1975, "The Role of Salt in Whitecap Persistence," Deep Sea Res., Vol. 22, 653.

A. Stogryn, 1972, "The Emissivity of Sea Foam at Microwave Frequencies," J. Geophys. Res., Vol. 77, No. 9, 1658.

M.-Y. Su, A.W. Green and Mark T. Bergin, 1984, "Experimental Studies of Water Wave Breaking," in *Gas Transfer at Water Surfaces*, W. Brutsaert and G.H. Jirka (eds.), D. Reidel, 211.

S.A. Thorpe, 1982, "On the clouds of bubbles formed by breaking wind waves in deep water, and their role in air-sea gas transfer," Phil. Trans. Royal Soc. Lond. A, Vol. 304, 155.

E. Van de Sande and J.M. Smith, 1972, "Eintragen von Luft in eine Flussigkeit durch einen Wasser Strahl," Chemie-Ing. Techn., Vol. 44, 1177.

E. Van de Sande and J.M. Smith, 1973, "Surface Entrainment of Air by High Velocity Water Jets." Chem. Eng. Sci., Vol. 28, 1161

E. Van de Sande J.M. Smith, 1976, "Jet Break-up and Air Entrainment by Low Velocity Turbulent Water Jets," Chem. Eng. Sci., Vol. 31, 219.

P.U. Volkart, 1982, "Self-Aerated Flow in Steep, Partially Filled Pipes," Proc. ASCE, Vol. 108 (HY9), 1029.

I.R. Wood, 1983, "Uniform Region of Self-Aerated Flow," Proc. ASCE, Vol. 109 (HY3), 447.

U23216

DEPARTMENT OF THE NAVY

NAVAL RESEARCH LABORATORY
Washington, D.C. 20375-5000

OFFICIAL BUSINESS
PENALTY FOR PRIVATE USE, $300

THIRD-CLASS MAIL
POSTAGE & FEES PAID
USN
PERMIT No. G-9